Isotopic production cross section of fragments in ^{56}Fe + p and ^{136}Xe(^{124}Xe) + Pb reactions over an energy range from 300A to 1500A MeV

Fu-Hu Liu[1,2,*] and Jun-Sheng Li[1]
[1]*Shanxi University, Taiyuan, Shanxi 030006, People's Republic of China*
[2]*McGill University, Montréal, Québec H3A 2T8, Canada*
(Received 13 August 2008; published 2 October 2008)

Using a unified description on multiplicity distributions of final-state particles, the spallation residues in ^{56}Fe + p reactions and fragmentation products in ^{136}Xe(^{124}Xe) + Pb reactions at intermediate energy and at the low end of high energies are studied. The isotopic production cross sections of fragments produced in the reactions are calculated by using a multisource ideal gas model. Each source contributes multiplicity-like distribution of neutrons like a radioactive object.

DOI: 10.1103/PhysRevC.78.044602 PACS number(s): 28.60.+s, 25.40.Sc, 25.40.Ep

I. INTRODUCTION

The spallation cross sections of nuclides such as Fe have been historically studied to understand the production, propagation, and composition of cosmic rays [1–6]. When propagating in the Galaxy, primary cosmic rays pass through the interstellar medium and some of them fragment into secondary cosmic rays. The secondary cosmic rays have chances to suffer further spallation. As a result of multispallation during propagation, the measured compositions of cosmic rays are a combination of different multispallations. Consequently, investigations of spallation cross sections of nuclides are very important for the understanding of cosmic-ray composition.

The investigations of spallation reactions are also important in the planning of spallation neutron sources and accelerator-driven subcritical reactors systems considered for the transmutation of nuclear waste [7]. Spallation reactions can also be used to understand nuclear reaction mechanisms to test the validity of various models at intermediate energy and at the low end of high energies. Investigations of spallation reactions are the best and usually the only way to collect a comprehensive set of high-quality spallation data regarding the productions of neutrons, light charged particles, and residual nuclei [7–10]. In the past years, spallation reactions and neutron-rich and neutron-poor isotopes were widely studied by nuclear physicists [11–20].

Recently, Villagrasa-Canton *et al.* [21] reported new and detailed experimental results concerning the isotopic production cross sections of spallation residues in the reaction ^{56}Fe + p for five energies of the iron beam (1500A, 1000A, 750A, 500A, and 300A MeV). Henzlova *et al.* [22] reported experimental investigation of the residues produced in the ^{136}Xe + Pb and ^{124}Xe + Pb fragmentation reactions at 1000A MeV. Here we are interested in the analysis of the isotopic production cross sections because of their importance in the investigations of cosmic-ray composition, nuclear spallation properties, nuclear reaction mechanisms, and technological applications. In this paper, we will use a unified description that was proposed in our recent work [23] on multiplicity distributions of final-state particles in different collision systems to study the isotopic production cross sections of fragments produced in ^{56}Fe + p and ^{136}Xe(^{124}Xe) + Pb reactions.

II. THE MODEL

In our recent work [23], a unified formula was proposed to describe the multiplicity distributions of final-state particles produced in e^+e^-, pp, $p\bar{p}$, e^+p, p-nucleus, and nucleus-nucleus collisions at high energies. If we regard the neutron number in a nuclide as like the neutron multiplicity in a final state, the unified formula can be used to analyze the isotopic production cross sections of fragments. The following description is a shortened and simplified version of the model of Ref. [23].

According to our multisource ideal gas model [24–26], many emission sources of particles and fragments are assumed to form in intermediate- and high-energy collisions. According to different interaction mechanisms or event samples, the sources are divided into l groups (subsamples). The source number in the jth group is assumed to be m_j. Each source contributes multiplicity distribution like a radioactive object; that is, the multiplicity (n_{ij}) distribution contributed by the ith source in the jth group is given by an exponential distribution,

$$P_{ij}(n_{ij}) = \frac{1}{\langle n_{ij}\rangle}\exp\left(-\frac{n_{ij}}{\langle n_{ij}\rangle}\right), \tag{1}$$

where $\langle n_{ij}\rangle = \int n_{ij}P_{ij}(n_{ij})dn_{ij}$ is the mean multiplicity contributed by the ith source in the jth group. Generally, we assume $\langle n_{1j}\rangle = \langle n_{2j}\rangle = \cdots = \langle n_{m_jj}\rangle$. The neutron multiplicity-like (i.e., neutron number N) distribution contributed by the jth group is then given by the folding of m_j exponential functions; that is, we have an Erlang distribution

$$P_j(N) = \frac{N^{m_j-1}}{(m_j-1)!\langle n_{ij}\rangle^{m_j}}\exp\left(-\frac{N}{\langle n_{ij}\rangle}\right). \tag{2}$$

In a Monte Carlo calculation, let R_{ij} denote a random variable in [0,1]. According to Eq. (1), we have

$$n_{ij} = -\langle n_{ij}\rangle \ln R_{ij}. \tag{3}$$

*fuhuliu@163.com; liufh@mail.sxu.cn

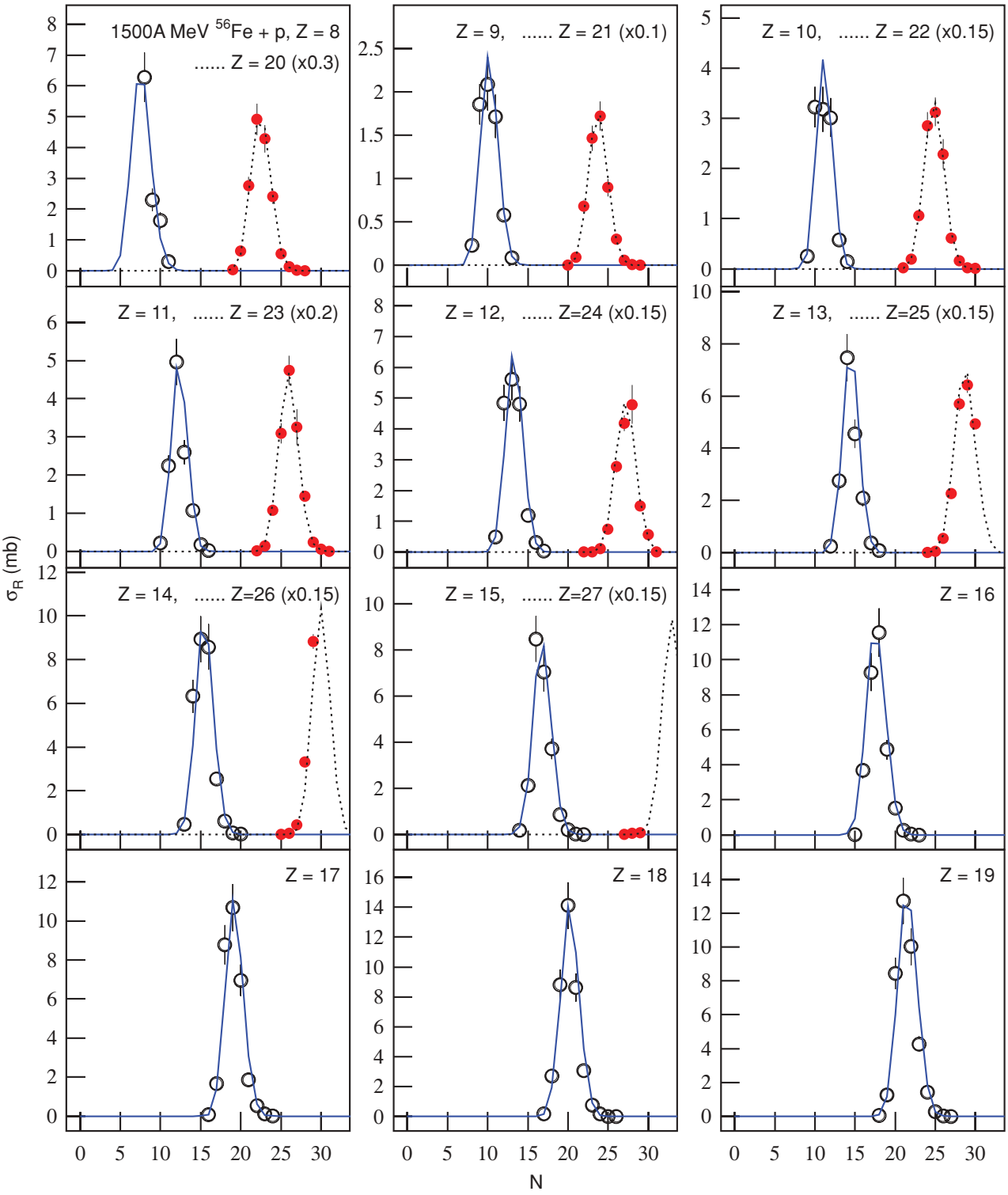

FIG. 1. (Color online) Isotopic production cross sections of fragments produced in ^{56}Fe + p reactions at 1500A MeV. The circles represent the experimental data of Villagrasa-Canton *et al.* [21]. The curves are our calculated results.

The neutron number can be obtained by

$$N = -\sum_{i=1}^{m_j} \langle n_{ij} \rangle \ln R_{ij} \tag{4}$$

owing to it being the folding of m_j exponential functions. The number distribution of neutrons for a given element is obtained by a statistical method. The isotopic production cross sections (σ_R) of fragments are directly proportional to the number distribution of neutrons. Generally speaking, $j = 1$

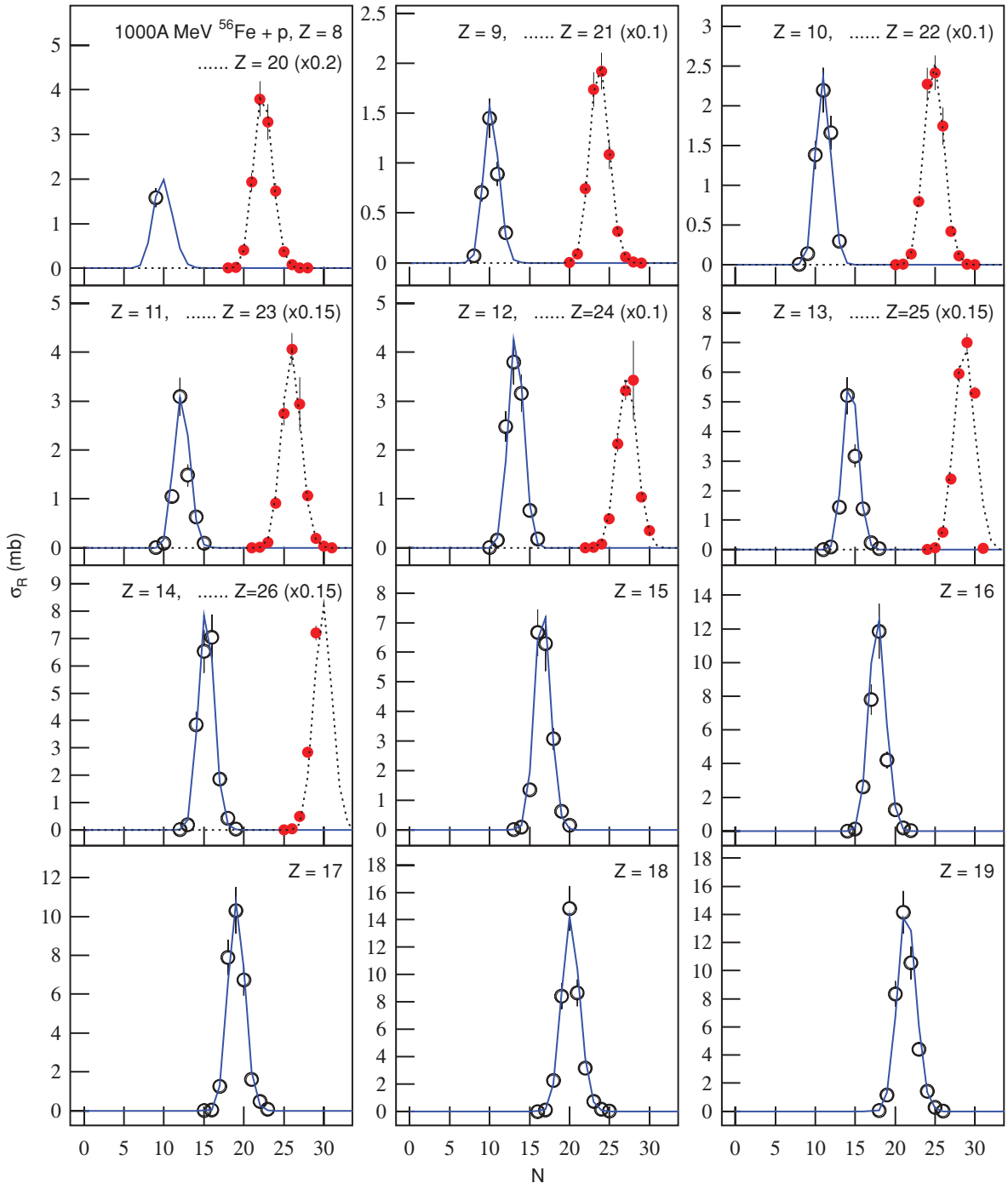

FIG. 2. (Color online) Same as Fig. 1, but showing the results at 1000A MeV.

for a given element. In the case of $j > 1$, we have to consider the relative weight for each j [23].

In this discussion, m_j denotes the source number in the jth group. The present model does not specify what the sources are. In the framework of a combination model of constituent quarks and Landau hydrodynamics [27,28], we may regard the sources as quarks and gluons in the case of m_j being a large value. If m_j is a small value, we may regard the sources as nucleons or nucleon clusters. In the framework of a two-stage gluon model or a gluon dominance model [29–31], the sources can be regarded as active gluons and evaporated gluons.

III. COMPARISONS WITH EXPERIMENTAL DATA

The isotopic production cross sections of fragments produced in $^{56}\mathrm{Fe} + p$ reactions at 1500A MeV are shown in Fig. 1. The circles represent the experimental data of Villagrasa-Canton *et al.* [21] for different charge numbers (Z)

TABLE I. Values of $\langle n_{i1}\rangle$, m_1, and χ^2/dof corresponding to the fits in Fig. 1.

Z	$\langle n_{i1}\rangle$	m_1	χ^2/dof	Z	$\langle n_{i1}\rangle$	m_1	χ^2/dof
8[a]	0.163	50	0.399	18	0.059	352	0.152
9	0.095	113	0.409	19	0.059	374	0.174
10	0.074	158	0.175	20	0.058	397	0.064
11	0.066	195	0.141	21	0.051	476	0.120
12	0.072	192	0.143	22	0.054	470	0.042
13	0.063	238	0.238	23	0.050	529	0.098
14	0.069	232	0.215	24	0.050	554	0.184
15	0.066	262	0.152	25	0.051	573	0.252
16	0.072	252	0.119	26[a]	0.037	825	1.020
17	0.057	346	0.181	27[a]	0.039	858	0.639[b]

[a]These parameter values are not included in Fig. 6 owing to the lack of partial data.
[b]The value of χ^2 is given instead of χ^2/dof.

and neutron numbers. The data for $Z = 20$–27 are scaled by different factors as marked in the figure. The curves are our calculated results. For each group with a given Z, there are two free parameters ($\langle n_{i1}\rangle$ and m_1) and a normalization constant. The values of $\langle n_{i1}\rangle$ and m_1 obtained by fitting the experimental data are given in Table I with the resulting χ^2 per degree of freedom (χ^2/dof). When the number of experimental points is less than four, the value of χ^2 is given instead of χ^2/dof. One can see that the model well describes the experimental data.

Figures 2–5 present the isotopic production cross sections of fragments produced in $^{56}\mathrm{Fe} + p$ reactions at $1000A$, $750A$, $500A$, and $300A$ MeV, respectively. The symbol definitions are as in Fig. 1. The fitted model parameter values are given in Tables II–V, respectively. In the calculation of χ^2/dof, the last point for $Z = 25$ is not included. Once more the model well describes the experimental data.

Figure 6 displays the dependencies of parameter values on incident energy and fragment charge number. One can see that

TABLE II. Values of $\langle n_{i1}\rangle$, m_1, and χ^2/dof corresponding to the fits in Fig. 2.

Z	$\langle n_{i1}\rangle$	m_1	χ^2/dof	Z	$\langle n_{i1}\rangle$	m_1	χ^2/dof
8[a]	0.124	84	0.000[b]	18	0.054	383	0.099
9	0.072	149	0.033	19	0.054	407	0.143
10	0.067	172	0.048	20	0.052	441	0.105
11	0.064	199	0.238	21	0.051	476	0.263
12	0.058	238	0.088	22	0.054	470	0.057
13	0.050	299	0.174	23	0.050	529	0.093
14	0.052	304	0.202	24	0.050	554	0.120
15	0.048	357	0.174	25	0.051	573	0.174[c]
16	0.050	366	0.207	26[a]	0.038	801	0.852
17	0.049	400	0.085				

[a]These parameter values are not included in Fig. 6 owing to the lack of partial data.
[b]The value of χ^2 is given instead of χ^2/dof.
[c]The last point is not included in the calculation of χ^2/dof.

TABLE III. Values of $\langle n_{i1}\rangle$, m_1, and χ^2/dof corresponding to the fits in Fig. 3.

Z	$\langle n_{i1}\rangle$	m_1	χ^2/dof	Z	$\langle n_{i1}\rangle$	m_1	χ^2/dof
8[a]	0.166	52	0.012[b]	18	0.046	449	0.141
9	0.054	196	0.069	19	0.047	467	0.200
10	0.055	208	0.168	20	0.049	471	0.079
11	0.048	263	0.286	21	0.047	518	0.152
12	0.057	245	0.073	22	0.050	508	0.035
13	0.047	318	0.214	23	0.044	599	0.271
14	0.049	324	0.252	24	0.040	691	0.639
15	0.045	382	0.164	25	0.049	596	0.120[c]
16	0.046	399	0.157	26[a]	0.038	801	0.815
17	0.045	436	0.156	27[a]	0.039	858	0.790[b]

[a]These parameter values are not included in Fig. 6 owing to the lack of partial data.
[b]The value of χ^2 is given instead of χ^2/dof.
[c]The last point is not included in the calculation of χ^2/dof.

TABLE IV. Values of $\langle n_{i1}\rangle$, m_1, and χ^2/dof corresponding to the fits in Fig. 4.

Z	$\langle n_{i1}\rangle$	m_1	χ^2/dof	Z	$\langle n_{i1}\rangle$	m_1	χ^2/dof
10[a]	0.118	92	0.051[b]	19	0.054	407	0.088
11	0.049	269	0.027	20	0.048	480	0.069
12	0.044	321	0.278	21	0.047	518	0.081
13	0.045	335	0.062	22	0.050	508	0.082
14	0.044	367	0.328	23	0.043	611	0.368
15	0.051	338	0.070	24	0.039	702	0.735
16	0.046	399	0.107	25	0.049	594	0.107[c]
17	0.046	427	0.059	26[a]	0.038	801	1.083
18	0.050	414	0.064	27[a]	0.039	858	1.050

[a]These parameter values are not included in Fig. 6 owing to the lack of partial data.
[b]The value of χ^2 is given instead of χ^2/dof.
[c]The last point is not included in the calculation of χ^2/dof.

TABLE V. Values of $\langle n_{i1}\rangle$, m_1, and χ^2/dof corresponding to the fits in Fig. 5.

Z	$\langle n_{i1}\rangle$	m_1	χ^2/dof	Z	$\langle n_{i1}\rangle$	m_1	χ^2/dof
10[a]	0.101	108	0.050[b]	19	0.051	433	0.074
11	0.059	218	0.046[b]	20	0.049	471	0.052
12	0.038	374	0.166	21	0.047	518	0.072
13	0.053	291	0.038	22	0.047	541	0.090
14	0.046	353	0.118	23	0.043	615	0.105
15	0.044	397	0.150	24	0.045	612	0.547
16	0.047	393	0.075	25	0.049	594	0.092[c]
17	0.046	427	0.044	26[a]	0.042	724	0.669
18	0.047	441	0.112	27[a]	0.046	724	1.344[b]

[a]These parameter values are not included in Fig. 6 owing to the lack of partial data.
[b]The value of χ^2 is given instead of χ^2/dof.
[c]The last point is not included in the calculation of χ^2/dof.

TABLE VI. Values of $\langle n_{i1}\rangle$, m_1, and χ^2/dof corresponding to the fits in Fig. 7.

Z	$\langle n_{i1}\rangle$	m_1	χ^2/dof	Z	$\langle n_{i1}\rangle$	m_1	χ^2/dof
5	0.061	107	1.880	31	0.068	554	0.158
6	0.101	74	0.219	32	0.067	584	0.142
7	0.062	139	0.904	33	0.068	595	0.086
8	0.100	99	0.315	34	0.073	571	0.156
9	0.100	114	0.040	35	0.065	662	0.119
10	0.086	142	0.370	36	0.069	642	0.109
11	0.080	167	0.603	37	0.069	660	0.165
12	0.080	178	0.503	38	0.068	688	0.183
13	0.073	213	0.468	39	0.063	765	0.130
14	0.072	230	0.574	40	0.066	750	0.196
15	0.074	243	0.359	41	0.063	805	0.323
16	0.073	261	0.192	42	0.079	660	0.427
17	0.072	283	0.215	43	0.090	595	0.422
18	0.081	267	0.139	44	0.100	553	0.240
19	0.084	273	0.127	45	0.097	585	0.249
20	0.077	311	0.070	46	0.100	585	0.223
21	0.071	355	0.082	47	0.120	502	0.182
22	0.064	412	0.089	48	0.118	525	0.198
23	0.063	440	0.200	49	0.143	447	0.258
24	0.066	436	0.138	50	0.164	403	0.413
25	0.073	410	0.118	51	0.178	388	0.393
26	0.070	445	0.102	52	0.199	360	1.135
27	0.063	514	0.125	53[a]	0.388	200	1.225
28	0.066	510	0.155	54[a,b]	0.435	200	1.602
29	0.068	516	0.167	55[a]	0.123	630	0.214
30	0.066	549	0.172	56[a]	0.086	855	0.021

[a]These parameter values are not included in Fig. 7 owing to the low statistics.

[b]This data set is fitted by $j = 2$. The other parameters are $\langle n_{i2}\rangle = 0.040$ and $m_2 = 2100$ with a weight of 0.75. Then the first group of parameters has a weight of 0.25.

TABLE VII. Values of $\langle n_{i1}\rangle$, m_1, and χ^2/dof corresponding to the fits in Fig. 8.

Z	$\langle n_{i1}\rangle$	m_1	χ^2/dof	Z	$\langle n_{i1}\rangle$	m_1	χ^2/dof
5	0.052	123	0.097	31	0.056	658	0.122
6	0.083	86	0.337	32	0.058	656	0.136
7	0.044	190	0.567	33	0.057	692	0.089
8	0.067	136	0.892	34	0.052	780	0.110
9	0.092	120	0.250	35	0.058	723	0.159
10	0.090	130	0.752	36	0.052	827	0.152
11	0.060	212	1.097	37	0.047	942	0.074
12	0.093	150	1.142	38	0.036	1270	0.236
13	0.055	271	0.678	39	0.047	995	0.153
14	0.067	240	0.354	40	0.048	1000	0.253
15	0.071	245	0.505	41	0.035	1410	0.153
16	0.058	318	0.164	42	0.032	1575	0.288
17	0.061	325	0.209	43	0.040	1290	0.147
18	0.058	360	0.210	44	0.038	1390	0.198
19	0.066	335	0.189	45	0.052	1045	0.203
20	0.078	300	0.327	46	0.045	1235	0.112
21	0.064	385	0.192	47	0.038	1525	0.306
22	0.066	390	0.172	48	0.038	1540	0.446
23	0.058	462	0.108	49	0.046	1300	0.187
24	0.063	445	0.141	50	0.049	1255	0.399
25	0.073	398	0.522	51	0.044	1440	0.572
26	0.056	542	0.084	52	0.051	1272	0.958
27	0.060	528	0.087	53[a]	0.210	340	1.889
28	0.056	587	0.075	54[a]	0.056	1260	1.494[b]
29	0.058	590	0.089	55[a]	0.036	1880	0.073
30	0.057	625	0.064				

[a]These parameter values are not included in Fig. 8 owing to the low statistics.

[b]The last (circled) point is not included in the calculation of χ^2/dof.

the parameter $\langle n_{i1}\rangle$ at intermediate energy ($700A$, $500A$, and $300A$ MeV) does not obviously depend on incident energy and fragment charge number. It falls into a narrow range consisting of two lines ($\langle n_{i1}\rangle = 0.059$ and 0.038). At the low end of high energies ($1500A$ and $1000A$ MeV), the parameter $\langle n_{i1}\rangle$ seems first to decrease with increasing Z and then to fall into the narrow range. However, it is hard to say there is a difference depending on the energy and Z because these differences looks just like statistical and method fluctuations. Throughout the concerned energy range, the parameter m_1 does not obviously depend on incident energy and increases with increasing Z. The product $\langle n_{i1}\rangle m_1$ increases linearly and strongly with increasing Z and does not depend on energy. These lines are uniformly described by $\langle n_{i1}\rangle m_1 = 1.17Z$ and are shown in the figure by plus or minus different amounts for clarity.

The isotopic production cross sections of fragments in ^{136}Xe + Pb and ^{124}Xe + Pb reactions at $1000A$ MeV are shown in Figs. 7 and 8, respectively. The symbols represent the experimental data of Henzlova *et al.* [22] for different Z and N. The data for some Z are scaled by different factors as marked in the figures. The fitted model parameter values are given in Tables VI and VII, respectively. In the calculation of χ^2/dof, the last (circled) point for $Z = 54$ in Fig. 8 is not included.

Figure 9 gives the dependencies of parameter values on projectile mass number and fragment charge number. One can see that the parameter $\langle n_{i1}\rangle$ falls mainly into a range consisting of two lines ($\langle n_{i1}\rangle = 0.101$ and 0.032). At high Z, the difference between the two kinds of reactions is obvious, and a few data points for ^{136}Xe + Pb reactions appear beyond the range. The parameter m_1 for ^{136}Xe + Pb reactions first increases with increasing Z and then decreases at high Z; and for ^{124}Xe + Pb reactions it increases with increasing Z throughout the whole Z range. The product $\langle n_{i1}\rangle m_1$ for both kinds of reactions increases with increasing Z, and a difference appears at high Z. The line is described by $\langle n_{i1}\rangle m_1 = 1.21Z$ for ^{124}Xe + Pb reactions.

IV. CONCLUSIONS AND DISCUSSIONS

In conclusion, the isotopic production cross sections of fragments produced in ^{56}Fe + p and ^{136}Xe(^{124}Xe) + Pb reactions at intermediate energy and at the low end of high energies are studied by using a unified formula. This formula was proposed by us to describe the multiplicity distributions of final-state

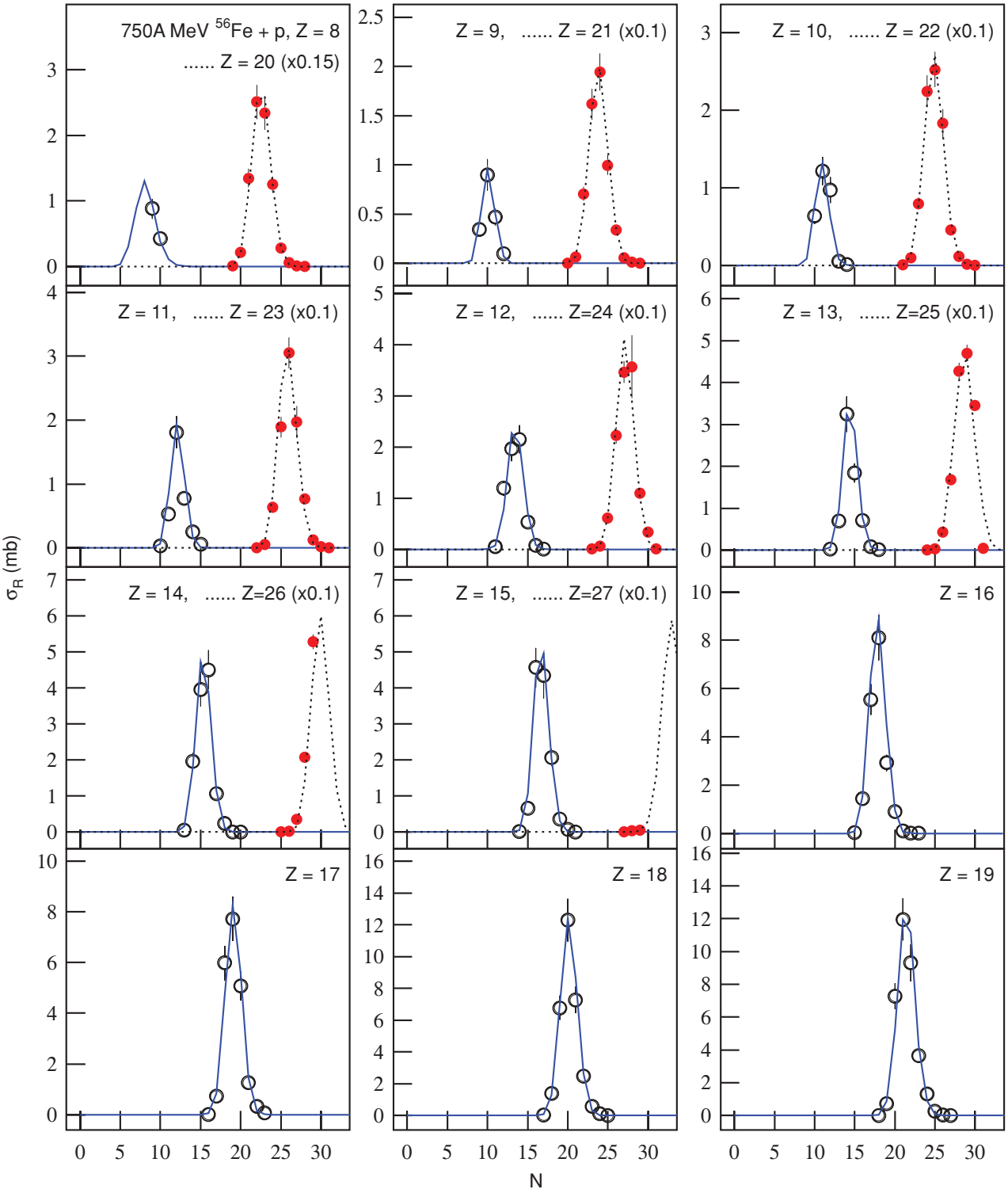

FIG. 3. (Color online) Same as Fig. 1, but showing the results at 750*A* MeV.

particles produced in "elementary" particle interactions and heavy-ion collisions. The neutron number in the isotope is regarded as multiplicity-like for neutrons. The isotopic production cross sections are treated as being directly proportional to the multiplicity-like distribution of neutrons.

In $^{56}\mathrm{Fe} + p$ reactions, at the low end of high energies, the parameter $\langle n_{i1} \rangle$ seems to depend on the energy and Z in

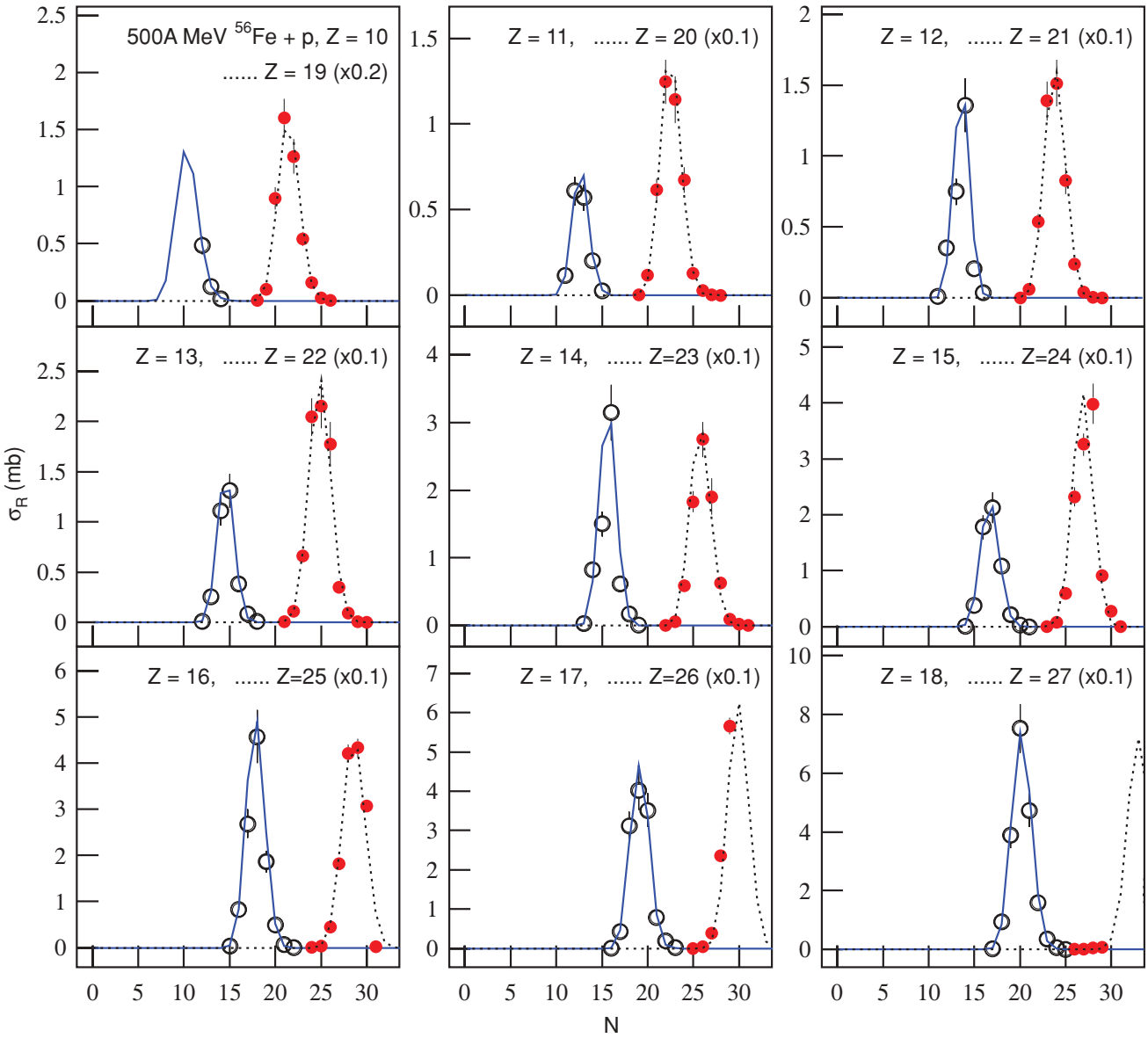

FIG. 4. (Color online) Same as Fig. 1, but showing the results at 500A MeV.

the low-Z range; it is independent of the energy and Z in the high-Z range. We cannot give a conclusion that there is a difference depending on the energy and Z because these differences looks just like statistical and method fluctuations. At intermediate energy, the parameter $\langle n_{i1}\rangle$ does not depend on the energy and Z throughout the whole concerned Z range. Especially, in the high-Z range, the values of parameter $\langle n_{i1}\rangle$ at the five energies studied fall into the same narrow range. The parameter m_1 and the product $\langle n_{i1}\rangle m_1$ increase with increasing Z and do not show an obvious dependence on the energy in the concerned energy range.

In ^{136}Xe + Pb and ^{124}Xe + Pb reactions at the low end of high energies, the parameter $\langle n_{i1}\rangle$ does not show an obvious dependence on the projectile mass number and fragment Z in the low-Z range, but it does show a dependence on the projectile mass number in the high-Z range. The parameter $\langle n_{i1}\rangle$, especially, for ^{136}Xe + Pb reactions shows a dependence on Z in the high-Z range. The parameter m_1 and the product $\langle n_{i1}\rangle m_1$ for the two kinds of reactions increase with increasing Z in the low-Z range and do not show an obvious dependence on the projectile mass number. In the high-Z range, the results for the two kinds of reactions are different. The parameter m_1 for the reaction ^{136}Xe + Pb decreases with increasing Z in this range. Obviously, the difference between the two kinds of reactions is caused by different projectile neutron numbers.

The difference at $Z > 35$ between ^{136}Xe and ^{124}Xe just indicates that we have more than one group contributing.

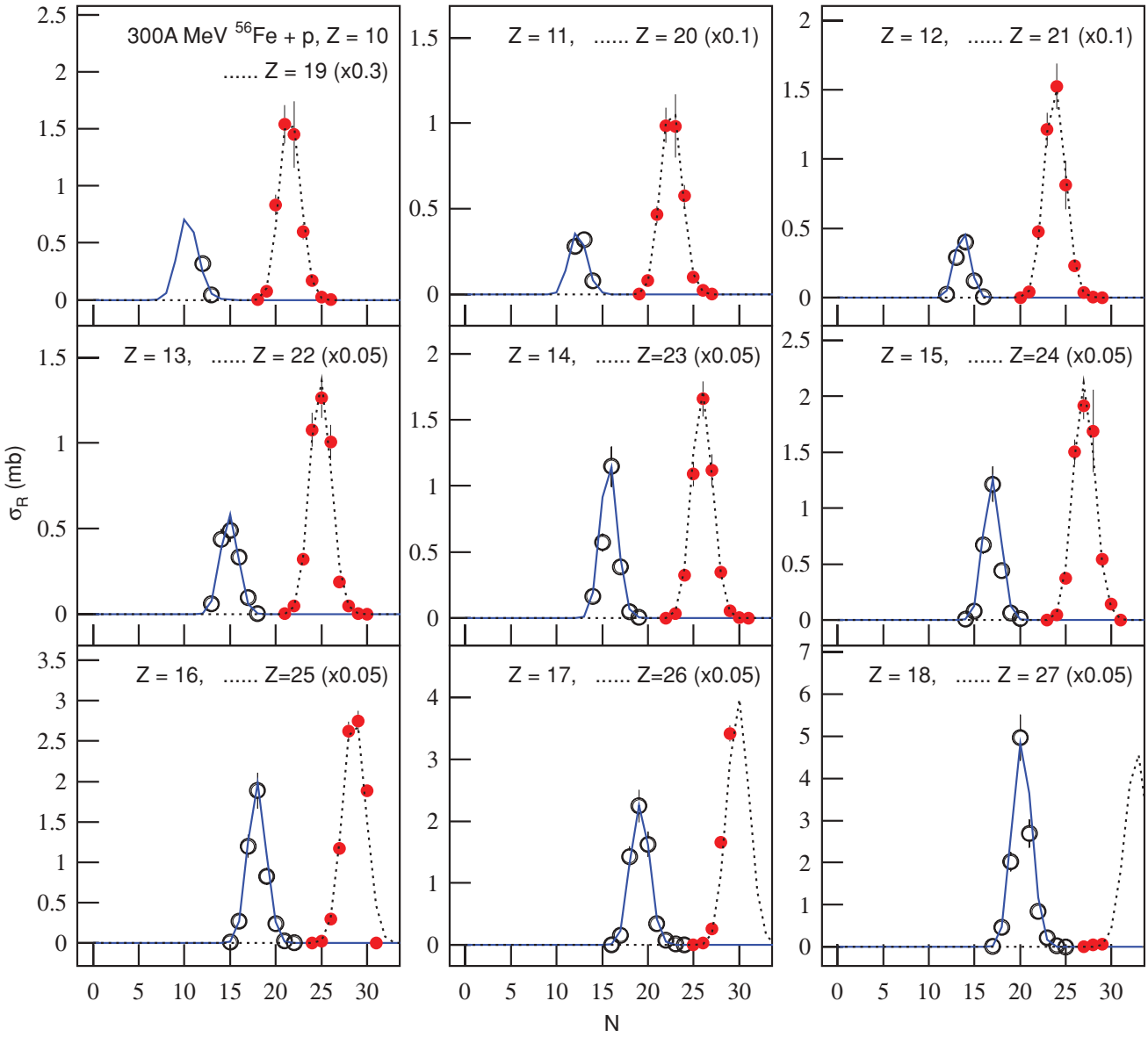

FIG. 5. (Color online) Same as Fig. 1, but showing the results at 300A MeV.

So, for example, ^{136}Xe may go down and be the same as ^{124}Xe if we take also into account m_2 (even m_3). The number of sources in a group may be the same, with some saturation number for a group, depending on Z, being attained. This may also explain a small excess in large Z for ^{136}Xe (except for errors and simply the lack of large Z values for lighter ^{124}Xe).

The product $\langle n_{i1}\rangle m_1$ is nothing but the mean N. This is no surprise because it increases in the same way as a function of Z in all reactions ($\sim 1.2Z$ being the same type reactions under study). This means that all the Z dependencies would coincide if we put them together, independent of the reaction species. The differences obtained for m_1 and $\langle n_{i1}\rangle$ in Fe + p reactions at different energies are probably due to statistical fluctuations, and that in heavier vs light Xe + Pb reactions looks due to more groups contributions. Otherwise, the values of m_1 look quite large, then this arise a question of: what are the "sources" thought of? This is indeed a question for us.

Finally, we would like to point out that the present work is a challenging investigation. We are concerned mainly with the description of multiplicity-like distributions of neutrons in isotopes emitted in nuclear reactions by a unified formula that describes the multiplicity distributions of final-state particles produced in high-energy collisions. Whether or not the behaviors of fitted parameters show a scaling law (dependence or similarity) on incident energy, fragment charge number, and projectile mass number is another subject.

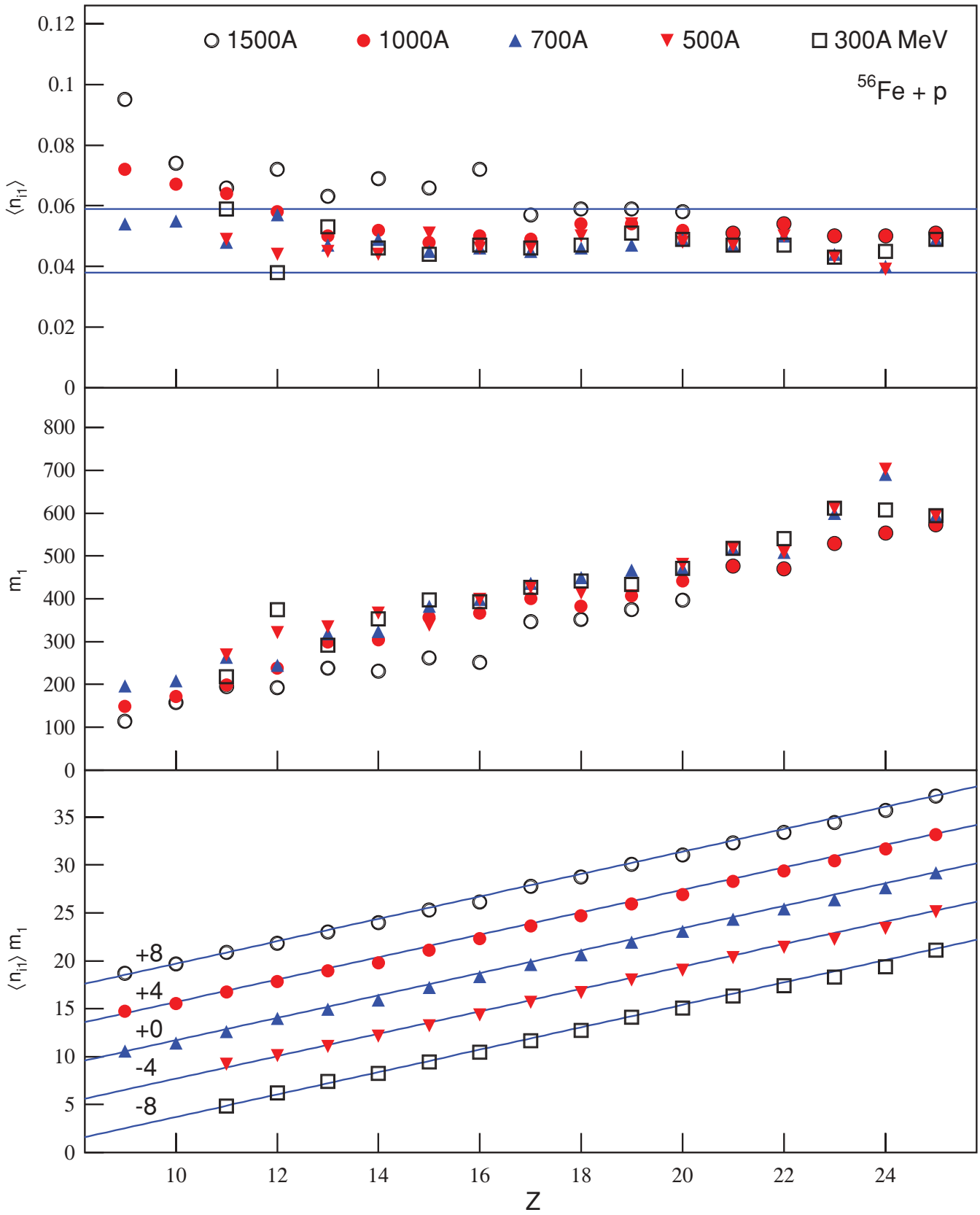

FIG. 6. (Color online) Correlations between $\langle n_{i1} \rangle$ and Z (top), m_1 and Z (middle), and $\langle n_{i1} \rangle m_1$ and Z (bottom) for $^{56}\mathrm{Fe} + p$ reactions at different energies.

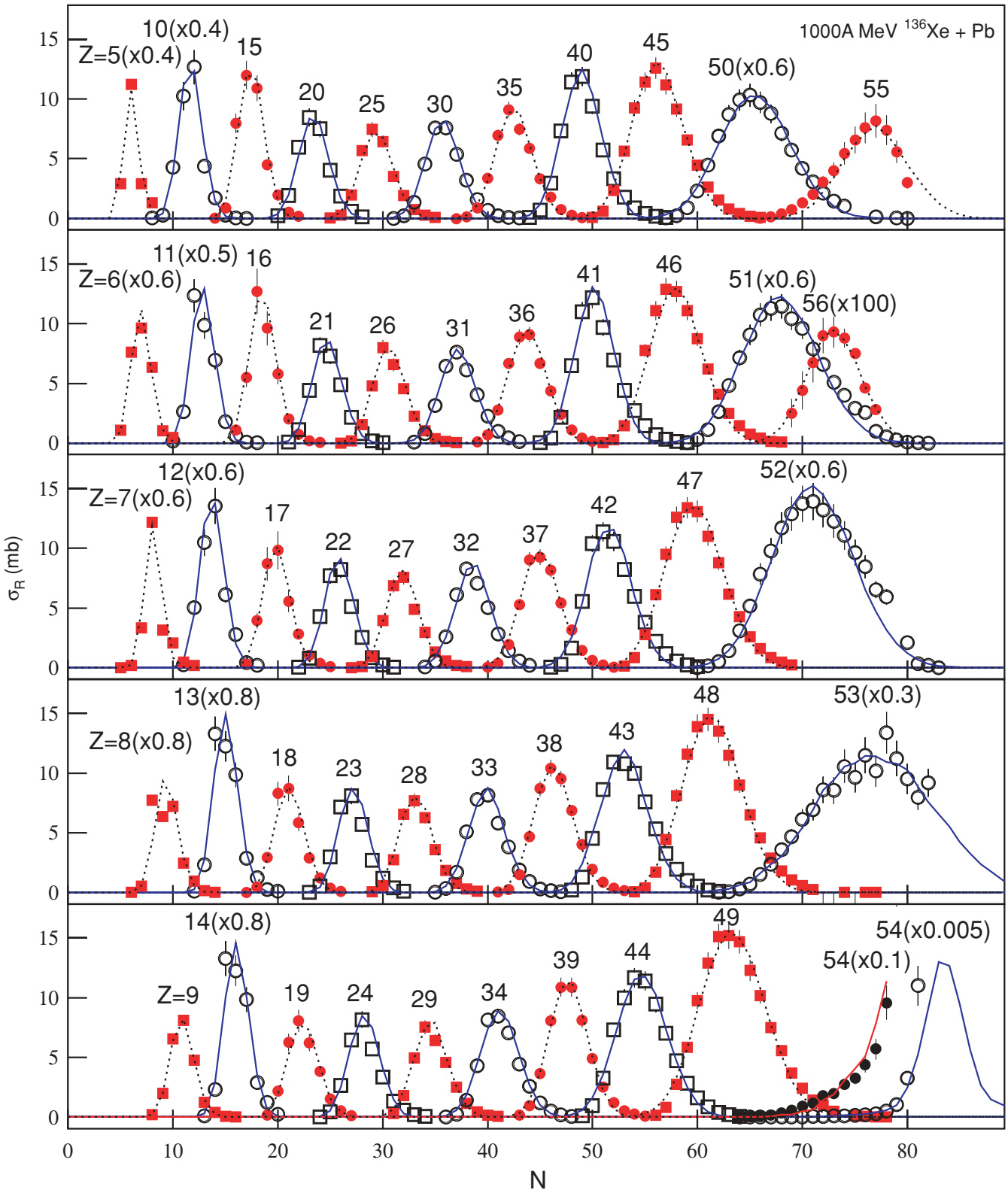

FIG. 7. (Color online) Isotopic production cross sections of fragments produced in ^{136}Xe + Pb reactions at 1000*A* MeV. The circles and squares represent the experimental data of Henzlova *et al*. [22]. The curves are our calculated results.

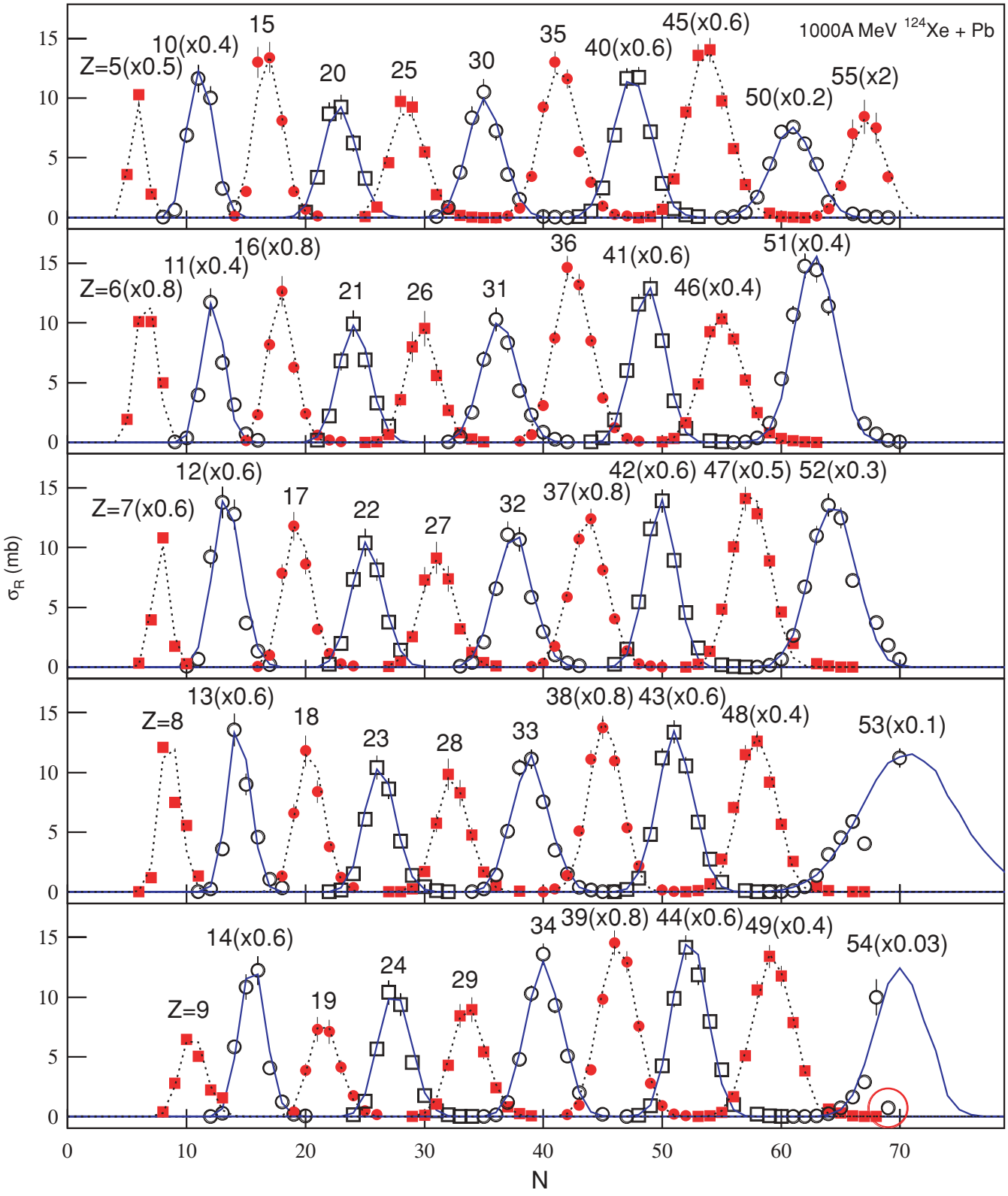

FIG. 8. (Color online) Same as Fig. 7, but showing the results for ^{124}Xe + Pb reactions.

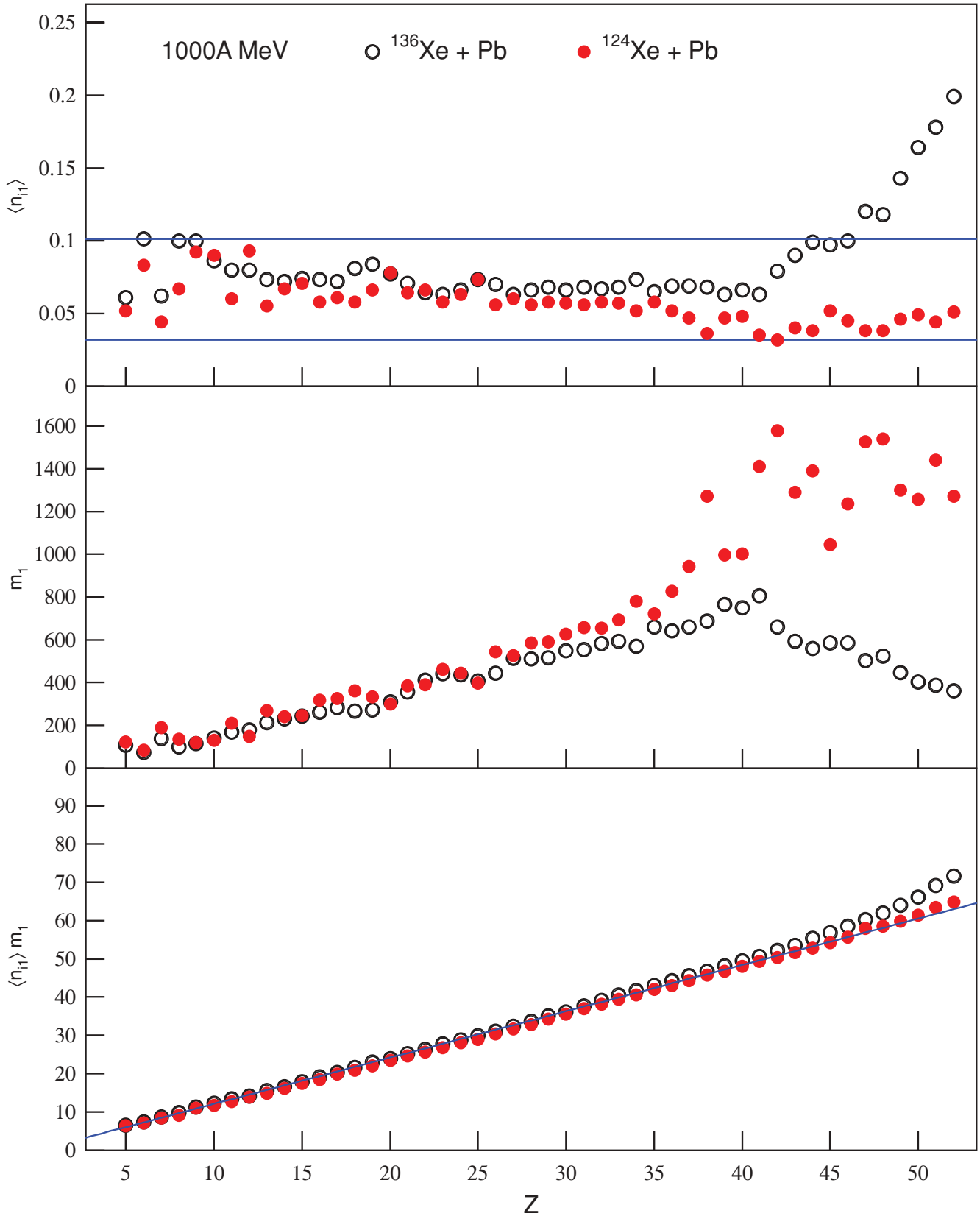

FIG. 9. (Color online) Correlations between $\langle n_{i1}\rangle$ and Z (top), m_1 and Z (middle), and $\langle n_{i1}\rangle m_1$ and Z (bottom) for ^{136}Fe + Pb and ^{124}Fe + Pb reactions at 1000A MeV.

ACKNOWLEDGMENTS

The authors thank Prof. Dr. Jean Barrette, Edward Sarkisyan, and Alexander Sakharov for their improvements to the manuscript. F.-H.L. thanks the members of the Physics Department of McGill University for their hospitality. This work was supported by the China Scholarship Council; the National Natural Science Foundation of China, Grant No. 10675077; the Shanxi Provincial Natural Science Foundation, Grant Nos. 2007011005 and 20051002; and the Shanxi Provincial Foundation for Returned Overseas Scholars.

[1] C. H. Tsao, R. Silberberg, A. F. Barghouty, L. Sihver, and T. Kanai, Phys. Rev. C **47**, 1257 (1993).
[2] W. R. Webber, J. C. Kish, and D. A. Schrier, Phys. Rev. C **41**, 533 (1990).
[3] C. Zeitlin, L. Heilbronn, J. Miller, S. E. Rademacher, T. Borak, T. R. Carter, K. A. Frankel, W. Schimmerling, and C. E. Stronach, Phys. Rev. C **56**, 388 (1997).
[4] G. D. Westfall, L. W. Wilson, P. J. Lindstrom, H. J. Crawford, D. E. Greiner, and H. H. Heckman, Phys. Rev. C **19**, 1309 (1979).
[5] W. R. Webber, J. C. Kish, J. M. Rockstroh, Y. Cassagnou, R. Legrain, A. Soutoul, O. Testard, and C. Tull, Astrophys. J. **508**, 940 (1998).
[6] W. R. Webber, J. C. Kish, J. M. Rockstroh, Y. Cassagnou, R. Legrain, A. Soutoul, O. Testard, and C. Tull, Astrophys. J. **508**, 949 (1998).
[7] J. P. Meulders, A. Koning, and S. Leray, edited by, HINDAS Final Report, EU Contract FIKW-CT-0031, 2005.
[8] C. M. Herbach, D. Hilscher, U. Jahnke, V. G. Tishchenko, J. Galin, A. Letourneau, A. Peghaire, D. Filges, F. Goldenbaum, L. Pienkowski, W U. Schroder, and J. Toke, Nucl. Phys. **A765**, 426 (1994).
[9] A. Letourneau, J. Galin, F. Goldenbaum, B. Lott, A. Peghaire, M. Enke, D. Hilscher, U. Jahnke, K. Nunighoff, D. Filges, R. D. Neef, N. Paul, H. Schaal, G. Sterzenbach, and A. Tietze, Nucl. Instrum. Methods B **170**, 299 (2000).
[10] S. Leray, F. Borne, S. Crespin, J. Frehaut, X. Ledoux, E. Martinez, Y. Patin, E. Petibon, P. Pras, A. Boudard, R. Legrain, Y. Terrien, F. Brochard, D. Drake, J. C. Duchazeaubeneix, J. M. Durand, S. I. Meigo, G. Milleret, D. M. Whittal, W. Wlazlo, D. Durand, C. Le Brun, F. R. Lecolley, J. F. Lecolley, F. Lefebvres, M. Louvel, C. Varignon, F. Hanappe, S. Menard, L. Stuttge, and J. Thun, Phys. Rev. C **65**, 044621 (2002).
[11] H. W. Barz, J. P. Bondorf, H. Schulz, L. N. Andronenko, A. A. Kotov, L. A. Vaishnene, and W. Neubert, Nucl. Phys. **A460**, 714 (1986).
[12] A. S. Hirsch, A. Bujak, J. E. Finn, L. J. Gutay, R. W. Minich, N. T. Porile, R. P. Scharenberg, B. C. Stringfellow, and F. Turkot, Phys. Rev. C **29**, 508 (1984).
[13] L. N. Andronenko, A. A. Kotov, L. A. Vaishnene, W. Neubert, H. W. Barz, J. P. Bondorf, R. Donangelo, and H. Schulz, Phys. Lett. **B174**, 18 (1986).
[14] V. E. Viola, K. Kwiatkowski, L. Beaulieu, D. S. Bracken, H. Breuer, J. Brzychczyk, R. T. de Souza, D. S. Ginger, W. C. Hsi, R. G. Korteling, T. Lefort T, W. G. Lynch, K. B. Morley, R. Legrain, L. Pienkowski, E. C. Pollacco, E. Renshaw, A. Ruangma, M. B. Tsang, C. Volant, G. Wang G, S. J. Yennello, and N. R. Yoder, Phys. Rep. **434**, 1 (2006).
[15] P. Napolitani, K.-H. Schmidt, and L. Tassan-Got, arXiv: 0806.3372v1 [nucl-ex].
[16] T. Gaitanos, H. Lenske, U. Mosel, Phys. Lett. **B663**, 197 (2008).
[17] M. Colonna, J. Rizzo, P. Chomaz, and M. Di Toro, Nucl. Phys. **A805**, 454c (2008).
[18] B. A. Bian, F. S. Zhang, and H. Y. Zhou, Nucl. Phys. **A807**, 71 (2008).
[19] N. Buyukcizmeci, A. S. Botvina, I. N. Mishustin, and R. Ogul, Phys. Rev. C **77**, 034608 (2008).
[20] J. Benlliure, M. Fernández-Ordóñez, L. Audouin, A. Boudard, E. Casarejos, J. E. Ducret, T. Enqvist, A. Heinz, D. Henzlova, V. Henzl, A. Kelic, S. Leray, P. Napolitani, J. Pereira, F. Rejmund, M. V. Ricciardi, K.-H. Schmidt, C. Schmitt, C. Stéphan, L. Tassan-Got, C. Volant, C. Villagrasa, and O. Yordanov, arXiv:0807.2851v1 [nucl-ex].
[21] C. Villagrasa-Canton, A. Boudard, J.-E. Ducret, B. Fernandez, S. Leray, C. Volant, P. Armbruster, T. Enqvist, F. Hammache, K. Helariutta, B. Jurado, M.-V. Ricciardi, K.-H. Schmidt, K. Sümmerer, F. Vivés, O. Yordanov, L. Audouin, C.-O. Bacri, L. Ferrant, P. Napolitani, F. Rejmund, C. Stéphan, L. Tassan-Got, J. Benlliure, E. Casarejos, M. Fernandez-Ordoñez, J. Pereira, S. Czajkowski, D. Karamanis, M. Pravikoff, J. S. George, R. A. Mewaldt, N. Yanasak, M. Wiedenbeck, J. J. Connell, T. Faestermann, A. Heinz, and A. Junghans, Phys. Rev. C **75**, 044603 (2007).
[22] D. Henzlova, K.-H. Schmidt, M. V. Ricciardi, A. Kelić, V. Henzl, P. Napolitani, L. Audouin, J. Benlliure, A. Boudard, E. Casarejos, J. E. Ducret, T. Enqvist, A. Heinz, A. Junghans, B. Jurado, A. Krása, T. Kurtukian, S. Leray, M. F. Ordóñez, J. Pereira, R. Pleskač, F. Rejmund, C. Schmitt, C. Stéphan, L. Tassan-Got, C. Villagrasa, C. Volant, A. Wagner, and O. Yordanov, arXiv:0801.3110v1 [nucl-ex].
[23] F. H. Liu, Nucl. Phys. **A810**, 159 (2008).
[24] F. H. Liu, Europhys. Lett. **63**, 193 (2003).
[25] F. H. Liu, N. N. Abd Allah, D. H. Zhang, and M. Y. Duan, Int. J. Mod. Phys. E **12**, 713 (2003).
[26] F. H. Liu, N. N. Abd Allah, and B. K. Singh, Phys. Rev. C **69**, 057601 (2004).
[27] E. K. G. Sarkisyan and A. S. Sakharov, CERN-PH-TH/2004-213, arXiv:hep-ph/0410324.
[28] E. K. G. Sarkisyan and A. S. Sakharov, AIP Conf. Proc. **828**, 35 (2006).
[29] E. Kokoulina, Acta Phys. Pol. B **35**, 295 (2004).
[30] E. S. Kokoulina and V. A. Nikitin, talk given at the XVII International Baldin Seminar "Relativistic Nuclear Physics and Quantum Chromodynamics," JINR, Dubna, Russia, Sept. 27–Oct. 2, 2004, arXiv:hep-ph/0502224.
[31] P. F. Ermolov, E. S. Kokoulina, E. A. Kuraev, A. V. Kutov, V. A. Nikitin, A. A. Pankov, I. A. Roufanov, and N. K. Zhidkov, talk given at the XVII International Baldin Seminar "Relativistic Nuclear Physics and Quantum Chromodynamics," JINR, Dubna, Russia, Sept. 27–Oct. 2, 2004, arXiv:hep-ph/0503254.